Optimization of the in-line X-ray phase-contrast imaging setup considering edge-contrast enhancement and spatial resolution*

JIA Quan-Jie(贾全杰) CHEN Yu(陈雨) LI Gang(黎刚) JIANG Xiao-Ming(姜晓明)[1)]

Institute of High Energy Physics, Chinese Academy of Sciences, Beijing 100049, China

Abstract: Employing the approximation theory based on refraction and the definition of the total point-spread-function of the imaging system, the variation in the edge contrast of simple model samples is discussed with different source-to-sample and sample-to-detector distances, which actually means different spatial resolutions of the imaging system. The experiments were carried out with the Beamline 4W1A imaging setup at the Beijing Synchrotron Radiation Facility for simple model and insect samples. The results show that to obtain clear phase-contrast images of biologic tissues for the X-ray in-line imaging setup, with determined parameters such as the size of the X-ray source, the pixel size of the detector and the fixed source-to-sample distance, there is a range of optimized sample-to-detector distances. The analysis method discussed in this article can be helpful in optimizing the setup of X-ray in-line phase-contrast imaging.

Key words: X-ray phase contrast imaging, edge-contrast enhancement, spatial resolution

PACS: 07.85.Qe, 42.25.Bs, 42.30.Va **DOI:** 10.1088/1674-1137/36/3/014

1 Introduction

Since Roentgen discovered the X-ray more than 100 years ago, the technique of X-ray imaging has been employed in many fields for the non-destructive characterization of the inner structure of objects. It was not until the late 1990s that hard X-ray phase-contrast imaging began to arouse considerable attention. As conventional techniques are based on the X-ray absorption properties of different materials, phase-contrast techniques aimed to exploit the phase shift between different parts and convert this into image contrast. In other words, contrast by phase-contrast imaging is related to δ, the decrement of the real part of the complex refractive index n, and the contribution to the phase shift of the X-ray waves. While absorption contrast by conventional imaging is related to β, the imaginary part of n, and causes an intensity decrease (absorption) of the X-ray waves. It has been found that for many biological tissues, δ is about three orders of magnitude larger than β for X-rays in the 10 to 100 keV range [1, 2]. Theoretically, a smaller scale of carcinomatous tissue may be observed with the phase contrast imaging techniques compared with the conventional ones. This means that if phase-contrast imaging techniques can be introduced successfully into clinical applications, they might promote the progress of modern medicine in early diagnosis cancers. Compared with other phase-contrast techniques such as diffraction-enhanced X-ray imaging [3–5] and X-ray imaging by interferometers [6, 7], which are based on the use of perfect crystals, in-line phase contrast X-ray imaging shows promise in clinical applications due to its simplicity.

The implementation of the in-line phase-contrast imaging set-up is mainly based on the optimization of the source-to-sample and sample-to-detector distances and, in principle, no additional optical elements are necessary. With this method, X-rays transmitted through the sample will propagate over a free-space distance between the sample and the detector. Variations in the thickness and X-ray refractive index of the sample lead to phase shifts for the X-ray waves passing through the sample, and after free propaga-

Received 16 May 2011, Revised 29 July 2011

∗ Supported by the National Natural Science Foundation of China (10475090)

1) Corresponding author, E-mail: jiangxm@ihep.ac.cn

tion of certain distance, these phase shifts are converted into detectable variations of intensity to form the phase-contrast image. The visual appearance of phase-contrast enhancement in the final image is the edge enhancement at the interfaces between components with different refractive indices. Due to the existence of a change in X-ray absorption across these interfaces, the effect of phase contrast is to provide a variable enhancement of the conventional absorption image. This kind of edge-enhanced contrast makes the edges between the soft tissues detectable, which is hardly observed by conventional absorption-based imaging.

According to the Fresnel-Kirchhoff integral [8], the one-dimensional intensity distribution of an image obtained by an in-line phase contrast imaging system with a monochromatic plane wave can be expressed as

$$I(x,z) = \frac{1}{\lambda z}\Big|\int \exp[\mathrm{i}\phi(x')-\mu(x')/2] \times \exp\left[\mathrm{i}\frac{\pi}{\lambda z}(x-x')^2\right]\mathrm{d}x'\Big|^2, \quad (1)$$

where z is the sample-to-detector distance, λ is the wavelength of the incident plane wave X-ray,

$$\phi(x') = -\frac{2\pi}{\lambda}\int \delta(x',z')\mathrm{d}z'$$

is the distribution of the X-ray phase shift passing through the sample as $\delta(x',z')$ being the decrement of the real part of the complex refractive index n of the sample, and $\mu(x')$ the z-projection of the linear attenuation coefficient of the sample. The contrast used to evaluate the relative difference between the intensity of the edge $I(x,z)$ and that of the local background I_{bg} is defined as [9]

$$\mathrm{Contrast}(x) = \frac{I(x,z)-I_{\mathrm{bg}}}{I_{\mathrm{bg}}}. \quad (2)$$

If the phase shift is small and the absorption effect can be ignored, as in the case of hard X-rays irradiating at soft biologic tissues, the phase contrast due to phase shift in the near-field regime could be simplified as proportional to the second derivative of phase distribution [10, 11]

$$C(x) = \frac{\lambda z}{2\pi}\phi''(x). \quad (3)$$

According to Eq. (3), in the near-field regime, phase contrast increases linearly with propagation distance z. This means that better phase contrast can be obtained by putting the detector far away from the sample. But in practical applications, the sizes of the X-ray source and the pixels of the detector cannot be ignored, which will blur the contrast seriously when increasing the distance z. Therefore, there is an optimum relation between the source-to-sample distance R_1 and the sample-to-detector distance R_2 for in-line phase contrast imaging.

In this work, the spatial resolution determined by parameters such as the intensity distribution of the X-ray source, the point-spread-function of the detector, and the source-to-sample and sample-to-detector distances will be considered for optimization of the in-line phase-contrast experimental setup. For a typical in-line experimental setup, as the size of the X-ray source, the pixel size of the detector and the source-to-sample distance are not normally possible to select, the sample-to-detector distance becomes an important parameter for optimizing the phase contrast. In fact, there are other restrictive factors on the imaging system, such as the sensitivity of the detector, the time of exposure, the radiation dosage, and so on, yet the influences of these factors are indirect and therefore will not be discussed in this article.

2 Quantitative analysis of edge-enhancement due to phase contrast for model samples

As the linear relationship of Eq. (3) between the contrast and the second derivative of the phase shift distribution is limited under the condition of weak phase objects [12] and is not suitable for many other cases, the approximation theory based on refraction [11, 13], which is also valid with large phase shifts, will be employed to depict the phase-contrast image by an ideal imaging system. For simplicity reasons only the phase contrast is focused on, while the effect of absorption contrast is ignored. According to that approximation, in the in-line phase-contrast images the X-ray intensity near the edge of the object can be deduced from Eq. (1) using the stationary phase method [8] and ignoring the interference effect between the points of the stationary phase due to the spread of the source.

$$I(x,z) = I_{\mathrm{i}}\sum_n \frac{1}{1+\dfrac{\lambda z}{2\pi}\phi''(\xi_n)}\exp[-\mu(\xi_n)], \quad (4)$$

where I_{i} is the intensity of the incident X-ray, $z = R_2R_1/(R_1+R_2) = R_2/M$ is the effective propagation distance [9] for the case of sphere-plane irradiation and is equivalent to the sample-to-detector distance for the case of plane-wave irradiation, and ξ_n denotes the position in the object plane from which the X-ray

propagates to the image plane to the position x. The relation between x and ξ_n is dominated by

$$x=\frac{\lambda z}{2\pi}\frac{\mathrm{d}\phi(\xi_n)}{\mathrm{d}\xi_n}+\xi_n,$$

which is called the stationary phase condition [8, 13].

For cylinder samples，in accordance with Eq. (4) and the stationary phase condition, the intensity distribution near the edge caused by phase shift can be expressed as [14]

$$I_{\mathrm{cylinder}}(x,z)=\begin{cases}1+\dfrac{1}{1+\dfrac{z\delta\sqrt{2r}}{2(r-\xi)^{3/2}}} & |x|>r\\ \dfrac{1}{1+\dfrac{z\delta\sqrt{2r}}{2(r-\xi)^{3/2}}} & |x|<r\end{cases}, \quad (5)$$

where r is the radius of the cylinder sample, ξ is relevant to x under the stationary phase condition, and the validity of Eq. (5) is limited under the condition $r\ll\sqrt{\lambda z}$.

According to Eq. (5), the maximum and minimum values of the intensity distribution near the edge of the cylinder sample can be calculated as 5/3 and 2/3, respectively, which are invariable with the increase of z, and the FWHMs of the peak and valley are $W_{\max}=1.5r^{1/3}z^{2/3}\delta^{2/3}$ and $W_{\min}=1.39r^{1/3}z^{2/3}\delta^{2/3}$, respectively [14]. The dotted line in Fig. 1 shows the simulated intensity distribution of a cylinder sample with a radius of 100 microns using Eq. (5).

Eq. (5) denotes an image with an ideal imaging system, i.e. an imaging system with a point-like source and an ideal detector of which the point-spread-function is an impulse-response-function. In the practical imaging system, the intensity distribution $s(x,y)$ of the X-ray source, and the point-spread-function $d(x,y)$ of the detector must be considered. The obtained image data with such imaging systems are actually the convolution of $s(x,y)$, $d(x,y)$ and $I(x,y)$. The "total point-spread-function" (PSF) of the imaging system, defined as the convolution of $s(x)$ and $d(x)$ referred to the object plane (which is just behind the object and normal to the X-ray incidence), can be expressed with the simplification of one-dimensional objects and the Gaussian form of functions with

$$s(x)=\frac{M-1}{M\sigma_{\mathrm{S}}\sqrt{\pi}}\exp\left[-\left(\frac{M-1}{M}\right)^2\frac{x^2}{\sigma_{\mathrm{S}}^2}\right]$$

and

$$d(x)=\frac{M}{\sigma_{\mathrm{D}}\sqrt{\pi}}\exp\left[-\frac{M^2x^2}{\sigma_{\mathrm{D}}^2}\right],$$

as the following [12]

$$\mathrm{PSF}(x,M)=\frac{1}{\sigma\sqrt{\pi}}\exp\left[-\frac{x^2}{\sigma^2}\right], \quad (6)$$

where

$$\sigma=\sqrt{\frac{\sigma_{\mathrm{D}}^2}{M^2}+\frac{(M-1)^2\sigma_{\mathrm{S}}^2}{M^2}},$$

$M=(R_1+R_2)/R_1$ is the geometric magnification of the imaging system, and R_1 and R_2 are the source-to-sample and sample-to-detector distances. σ_{S}, σ_{D} are the standard deviations of the intensity distribution of the source and the point-spread-function of the detector, respectively. Normally, $2\sqrt{\ln 2}\sigma$ characterizes the spatial resolution of the imaging system.

Thus, the intensity distribution of the image for these kinds of samples by the real imaging system can be expressed as

$$I_{\mathrm{real}}(x,z)=I_{\mathrm{cylinder}}(x,z)\otimes\mathrm{PSF}(x,M), \quad (7)$$

where the symbol "⊗" denotes the convolution product. In accordance with the properties of convolution, the PSF will expand the peaks of intensity distribution and lower the value of the maximum, which decreases the contrast of the image. As shown in Fig. 1, the dash-dotted and solid line illustrate the intensity distributions of a cylinder sample by the real imaging systems with σ_{S} equal to 300 and 1700 microns, respectively, while σ_{D} is equal to 13.2 microns.

It is obvious in Fig. 1 that the maximum intensity is reduced considerably due to the expansion effect of PSF, which results in a decrease of edge-enhanced contrast. Smaller σ_{S} and σ_{D} result in a sharper PSF function, and then a smaller decrease in the edge-enhanced contrast, which reveals the key importance of dedicated small X-ray sources and high-resolution detectors in phase-contrast imaging techniques.

Since the convolution in Eq. (7) is not able to be expressed as a simple closed-form, we employed the parameter ratio defined in Eq. (8) to evaluate the influence of the effective distance z on the edge-enhanced phase contrast.

$$C(\sigma,r,z\delta)\propto W/\sigma, \quad (8)$$

where $W=r^{1/3}z^{2/3}\delta^{2/3}$ is the characteristic parameter relevant to $W_{\max}$ or $W_{\min}$ obtained from Eq. (5).

Such a parameter ratio is normally used in the consideration of the properties of the convolution product of two functions–one takes the form of the PSF,

$$\frac{1}{\sigma\sqrt{\pi}}\exp\left[-\frac{x^2}{\sigma^2}\right],$$

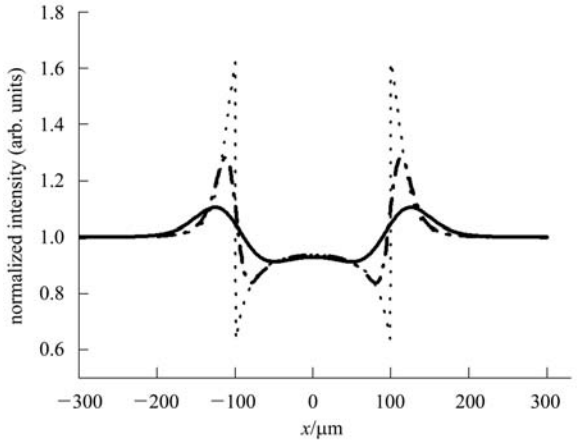

Fig. 1. Simulated intensity distribution of the phase contrast images of a cylinder sample by the approximation theory based on refraction. The radius of the simulation sample is 100 microns, the incident X-ray energy is 12.4 keV, the value of δ is 10^{-6} and the effective distance z is 1 meter. The thin dotted line denotes the ideal intensity distribution $I_{\rm cylinder}\,(x,z)$ obtained from Eq. (5), the dash-dotted line and solid line denote $I_{\rm real}\,(x,z)$ obtained from Eq. (7), with $\sigma_{\rm S}$ equal to 300 and 1700 microns, respectively, while $\sigma_{\rm D}$ is equal to 13.2 microns.

and the other takes the form $\exp\left[-\dfrac{x^2}{W^2}\right]$. It can be found that the maximum of the convolution product of these two functions is $W/\sqrt{\sigma^2+W^2}$, which is approximately proportional to W/σ if the value of W/σ is relatively small. The parameter as in Eq.(8) may be roughly used to estimate the tendency of the edge-contrast enhancement of the cylinder samples, but cannot provide the exact contrast value and should be constrained within the condition of the relatively small value of W/σ.

3 The experiment and discussions of in-line phase-contrast imaging at the Beamline 4W1A at the Beijing Synchrotron Radiation Facility

The in-line imaging experiments are carried out on Beamline 4W1A at the Beijing Synchrotron Radiation Facility (BSRF). The X-ray source is a single-period wiggler, of which the standard deviation of the horizontal size is about 1700 microns and the vertical one about 300 microns. That means this imaging system will provide two different PSF values simultaneously at the vertical and horizontal directions, respectively. The pixel size of the CCD detector used is about 11 microns, from which the standard deviation charactering the PSF of the detector can be derived as 13.2 microns approximately, in accordance with the Nyquist theorem. During the imaging experiments, the source-to-sample distance R_1 was fixed at 45 meters and the images were taken at different sample-to-detector distances R_2, which were much smaller than R_1.

The variances of the PSF of such imaging systems at certain different distance R_2 are listed in Table 1, along with the corresponding spatial resolutions. Shown in Fig. 2 is the spatial resolution of the imaging system versus R_2 with different source sizes and pixel sizes of the detector.

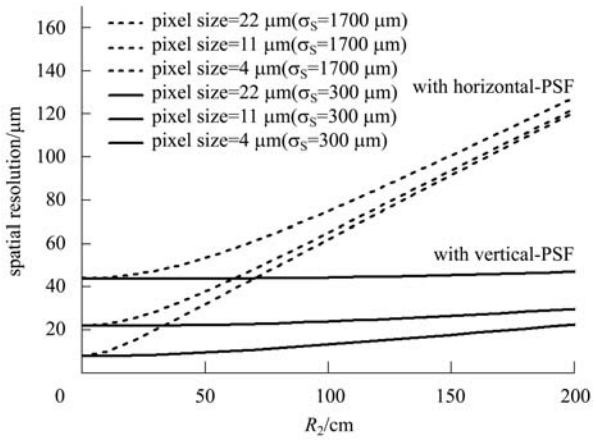

Fig. 2. Variation in spatial resolution due to different source sizes and changes in detector pixel size. The curve styles sequenced from top to bottom in the legend denote the curves plotted in the same sequence.

As shown in Fig. 2, the spatial resolution becomes worse with the increase in R_2 for either direction of the source. For the vertical direction ruled by the 300 microns source size, the degradation rate of the spatial resolution is very slow when R_2 increases, while for the horizontal direction the degradation rate is quick. As for the variation in spatial resolution caused by varying detector pixel sizes, it can be clearly seen from Fig. 2 that for a large ratio of source size to detector pixel size, the influence of pixel size on the spatial resolution is mainly dominated by the source property, while for a relatively small ratio the influence caused by detector pixel size becomes noticeable.

With this imaging setup, imaging experiments for two kinds of samples were carried out, one for the nylon threads as model samples, and the other for a kind of insect (anaxipha pallidula).

Table 1. The variance of the PSF of the imaging system and the spatial resolution at different sample-to-detector distances, R_2.

distance R_2/cm		14.0	45.5	85.0	115.5
PSF σ/μm	vertical direction	13.2	13.4	14.1	14.9
	horizontal direction	14.2	21.5	34.1	44.4
spatial resolution/μm	vertical direction	22.0	22.4	23.5	24.8
	horizontal direction	23.6	35.7	56.7	74.0

A set of nylon threads with different diameters were used as the cylinder model samples, with an incident X-ray energy of E=12 keV. The decrement of the real part of the refractive index for these kinds of nylon samples is $\delta_{12\ \mathrm{keV}} = 3.38\times10^{-6}$, and the threads with diameters of 440, 200 and 110 μm are studied. In the imaging experiments, the source-to-sample distance R_1 was kept at 45 m, and the images were obtained at different sample-to-detector distance R_2, changing from zero to 163 cm. Images of these nylon threads at four different sample-to-detector distances are shown in Fig. 3(a) as examples. The variations in the edge contrast of threads placed both vertically and horizontally are shown in Fig. 3(b), of which the data are obtained by intensity distributions acquired along the white lines marked in Fig. 3(a).

The experimental edge contrast plotted in Fig. 3(b) indicates that, as for the nylon threads that are placed vertically (which is imaged with the horizontal PSF), before the sample-to-detector distance R_2 reaches about 40 cm, the edge contrast increases rapidly with the increase in R_2. When R_2 exceeds 50 cm, the edge contrast no longer rises with the increase in R_2. For the nylon threads placed horizontally (which is imaged with the vertical PSF), within the adjustable range of R_2 for this experiment, the edge contrast maintains the tendency to increase quickly. Furthermore, for the nylon threads of different diameters placed in the same direction (vertical or horizontal), the edge contrast is relatively lower for the nylon thread with a smaller diameter at the same sample-to-detector distance R_2, but the tendency of edge contrast enhancement with the increase in R_2 is the same.

According to Eq. (8), with the parameters of the imaging setup, the tendency of edge contrast enhancement versus R_2 for samples of different diameters with the two different PSFs (two different sizes of the source along the vertical and horizontal directions, respectively) is plotted in Fig. 4. It is clearly shown in Fig. 4 that for the samples in the horizontal PSF case (with a source size of 1700 microns), when R_2 increases from zero, $C(\sigma, r, z\delta)$ grows rapidly and then slowly after R_2 >30 cm, and reaches maximum at $R_2 \approx$49 cm. This tendency is the same for the samples of different diameters, but with different contrast maximum values for different diameters, and the different maximum contrasts are almost the same as those obtained in the experiments as shown in Fig. 3(b). In the vertical PSF case (with a source size of 300 microns), the tendency of edge-contrast enhancement is also the same as that obtained from the experiment for horizontally placed nylon samples, and the edge-enhanced contrast values are much larger than those in the horizontal PSF case, which could be obtained by Eq. (8) with a smaller σ of the vertical PSF. In order to attain the same edge contrast value by a detector with definite sensitivity, as shown in Fig. 4 by the horizontal thick line of 0.08 contrast value, there are different minimum sample-to-detector distances for samples with different diameters, implying that the structures of different scales require a different sample-to-detector distance R_2 for detectable contrast determined by the sensitivity of the detector.

In general, the tendency of edge contrast to increase with the increase in R_2 is due to the competition between the increase in the peak width of edge intensity distribution and the increase in the variance of PSF. Firstly, according to Eq. (6), a smaller source size results in a smaller PSF σ, and so the expansion effect of PSF on the intensity distribution is less than that of a larger source size, thus leading to higher edge contrast. This is the result we got from both the analytic expression and the experiments shown in Figs. 4 and 5. Secondly, in the case of $R_2/R_1 \ll 1$, we get

$$\sigma \approx \sqrt{\sigma_{\mathrm{D}}^2 + \frac{R_2^2\sigma_{\mathrm{S}}^2}{R_1^2}},$$

and substituting it into Eq. (8), it can be found that the contrast $C(\sigma, r, z\delta)$ attains its maximum value at $R_{2\max} = \sqrt{2}R_1\sigma_{\mathrm{D}}/\sigma_{\mathrm{S}}$, which is about 49 cm for the horizontal PSF and 220 cm for the vertical PSF experimental setups. After $R_2 > R_{2\max}$, the increase in PSF will predominate in the competition and results in the decrease in edge-enhanced contrast with the increase in R_2. Thus, there exists an optimum

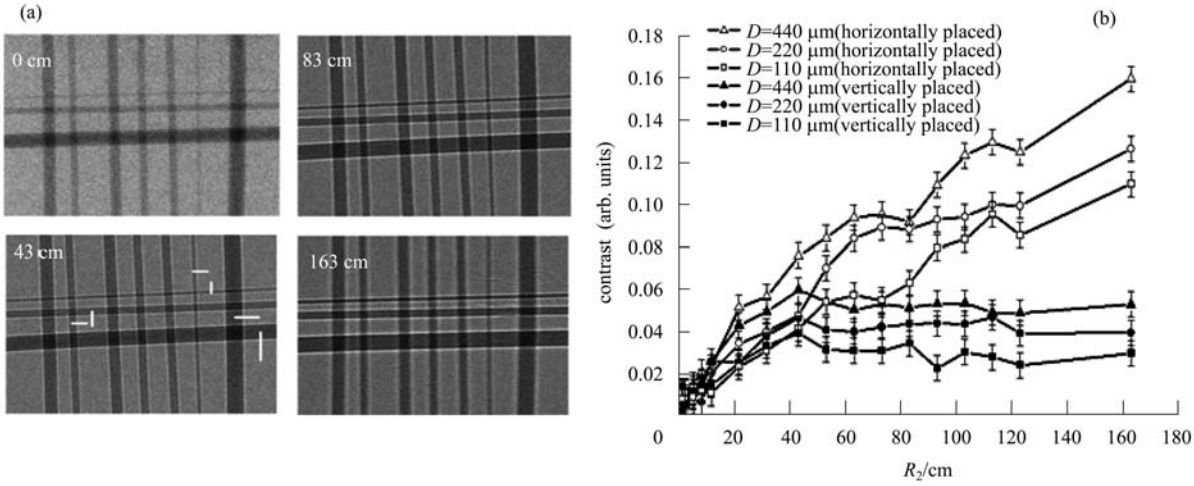

Fig. 3. (a) Images of a set of nylon threads obtained at four different sample-to-detector distances (with R_2=0, 43, 83 and 163 cm, respectively). There are six white lines shown in the image of R_2=43 cm, along which the intensity data are acquired for calculating the corresponding edge contrast used in (b). (b) Variation in the edge contrast of nylon threads with a variation in the sample-to-detector distance R_2. The hollow (horizontally placed) and solid (vertically placed) symbols denote the nylon threads placed along the horizontal and vertical direction, respectively, and the error bars are set with the assumption of Poisson statistical noises in each pixel.

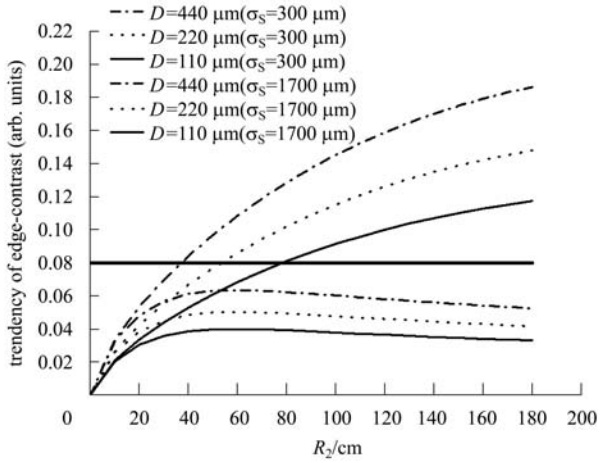

Fig. 4. The tendency of edge-contrast enhancement calculated by Eq. (8), which is defined for the evaluation of edge-enhanced contrast with the increase in sample-to-detector distance R_2. The curve styles sequenced from top to bottom in the legend denote the curves plotted in the same sequence, and the thick line indicates a certain level of edge contrast.

sample-to-detector distance for maximum edge-enhanced contrast. Thirdly, as the spatial resolution of the imaging system becomes degraded with the increase in R_2, certain constraints should be put on R_2 to clearly discern the detailed structure, though the increase in edge-enhanced contrast is maintained with the increase in R_2, that is to say that a compromise should be made between the edge contrast and the spatial resolution for specified samples.

Demonstrated in Fig. 5(a) are a series of images from an insect sample obtained using the same imaging system. The data plotted in Fig. 5(b) are obtained by the intensity distribution acquired along the black lines marked in Fig. 5(a) with the labels "a" and "b", denoting the vertical and horizontal structures, respectively. According to the curve of the edge contrast of structure "b" in Fig. 5(b), edge contrast grows slowly after R_2 exceeds 45 cm, which is similar to the foregoing discussion on the edge contrast of nylon threads placed vertically. The edge contrast curve of structure "a" maintains a fast-growing tendency like the nylon threads placed horizontally.

The locally enlarged images of the insect sample are shown in Fig. 6. In the image obtained at R_2=14 cm, the borders between the lumpy structures in the chest/back (as confined within the dashed-white-line circle marked in the image obtained at R_2=14 cm) of the insect are hard to identify, since the phase contrast is quite low at this distance and it is not possible for the absorption mechanism to provide clear contrast. When R_2 is at 45.5 cm, fine structures of the same part along both directions can be seen clearly. For the images obtained at R_2=85 and 115.5 cm, the borders along the vertical direction become very vague, but those along the horizontal direction are still quite legible.

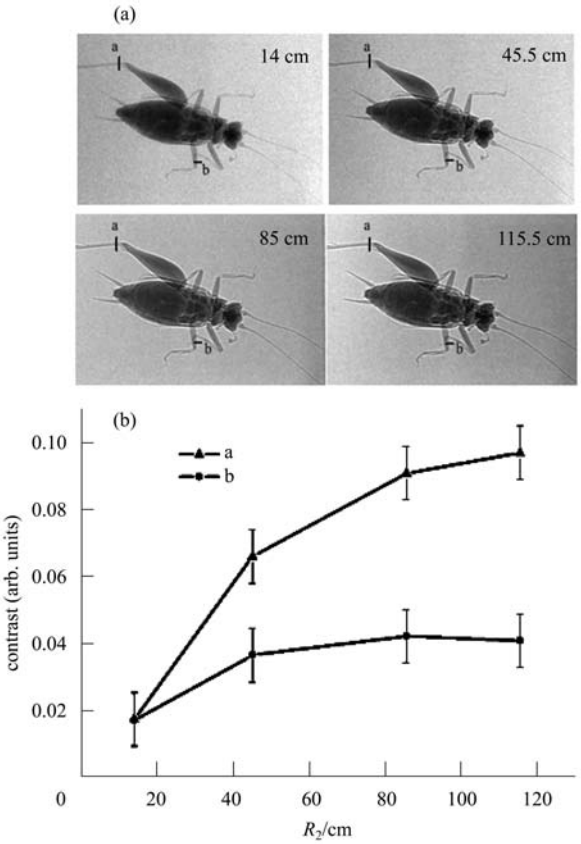

Fig. 5. (a) X-ray in-line phase contrast images of an insect (anaxipha pallidula) sample. The X-ray energy is E=12 keV, and the lines labeled "a" and "b" indicate the structures of which the tendency of edge contrast is discussed. (b) The variation in edge contrast for structures "a" and "b" with an increase in sample-to-detector distance R_2.

As mentioned before, such results can be explained by the tendency of edge contrast enhancement (as shown in Fig. 5(b)) together with the variation in spatial resolution (as listed in Table 1). For the vertical distributed structures, the edge contrast imaged with the horizontal PSF is almost unchanged after R_2 >45 cm, as shown in Fig. 5(b). While the spatial resolution for the source size of 1700 microns has been degraded as much as 56.7 microns at R_2=85 cm, and becomes even worse with the increase in R_2, as shown in Table 1. So the worse spatial resolutions make the image blur for the vertical distributed structures at R_2=85 and 115.5 cm. On the other hand, for the horizontal distributed structures, the edge contrast imaged with the vertical PSF grows obviously even at distances of R_2=115.5 cm or more, as shown in Fig. 5(b), and the spatial resolution for the source size of 300 microns is better than 30 microns in the whole range of R_2 <200 cm, as shown in Fig. 2. Both increasing contrast and good spatial resolution result in the images with more clear details for the horizontal distributed structures at R_2=85 and 115.5 cm.

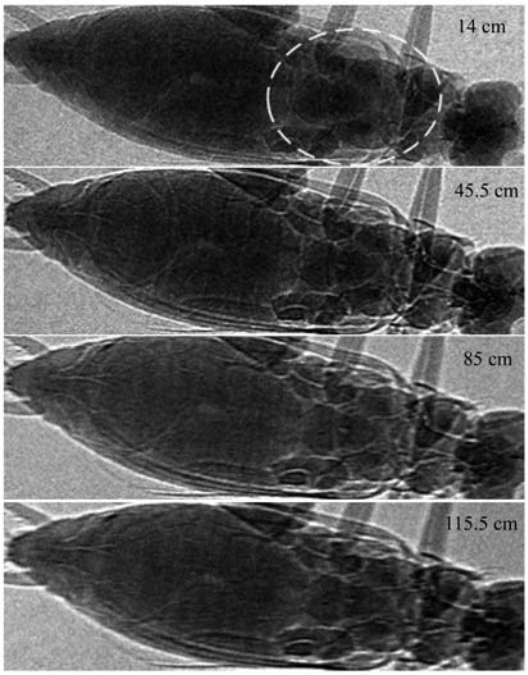

Fig. 6. The locally enlarged X-ray in-line phase contrast images of the insect body.

4 Conclusion

Using the approximation theory based on refraction with the Gaussian PSF of the imaging system, variations in the edge contrast of simple model samples are discussed with respect to the change in sample-to-detector distances R_2.

The trend of increasing edge contrast with the increase in R_2 is constrained by the PSF of the imaging system. To attain the detectable contrast determined by the sensitivity of the detector, different R_2 is required for the different structures in the samples. For the structures of the same geometric form, to a certain extent, the trend of edge contrast enhancement increasing with increasing R_2 is similar, and an optimum sample-to-detector distance for maximum edge-enhanced contrast exists. Meanwhile, as the spatial resolution gets worse with increasing R_2, a compromise between edge-enhanced contrast and spatial resolution is of great importance in order to clearly observe the specific details.

The authors would like to thank Prof. Zhu Peiping for some helpful discussions, and the staff of the BSRF imaging station for assistance in the imaging experiments.

References

1 WU Xi-Zeng, LIU Hong. J. X-Ray Sci. Technol., 2003, **11**(1): 33
2 ZHOU Shu-Ang et al. Phys. Medica, 2008, **24**(3): 129
3 Chapman D et al. Phys. Med. Biol., 1997, **42**(11): 2015
4 JIANG Xiao-Ming et al. HEP&NP, 2004, **28**(12): 1282 (in Chinese)
5 CHEN Yu et al. HEP&NP, 2007, **31**(10): 982(in Chinese)
6 Ando M, Hosoya S. An Attempt at X-ray Phase-Contrast Microscopy. In: Shinoda G, Kohra K, Ichinokawa T ed. Proc. 6$^{\text{th}}$ Intern. Conf., On X-ray Optics and Microanalysis. Tokyo: University of Tokyo Press, 1972. 63; Kakeda T et al. Acad. Radiol., 1995, **2**(9): 799
7 Momose A. Radiology, 2000, **217**(2): 593
8 Born M, Wolf E. Principles of Optics. 7th ed. Cambridge: Cambridge University Press, 1999. 425, 888
9 Nesterets Y I et al. Rev. Sci. Instrum., 2005, **76**(9): 093706-1
10 Pogany A et al. Rev. Sci. Instrum., 1997, **68**(7): 2774
11 Peterzol A et al. Med. Phys., 2005, **32**(12): 3617
12 Gureyev T E et al. Opt. Express, 2008, **16**(5): 3223
13 Monnin P et al. Med. Phys., 2004, **31**(6): 1372
14 Ishisaka A et al. Opt. Rev., 2000, **7**(6): 566